Sub-100-ps dynamics of the anomalous Hall effect at terahertz frequencies

T. J. Huisman,* R. V. Mikhaylovskiy, Th. Rasing, and A. V. Kimel
Radboud University, Institute for Molecules and Materials, 6525 AJ Nijmegen, The Netherlands

A. Tsukamoto
College of Science and Technology, Nihon University, 7-24-1 Funabashi, Chiba, Japan

B. de Ronde
MESA+ Institute for Nanotechnology, University of Twente, 7500 AE Enschede, The Netherlands

L. Ma, W. J. Fan, and S. M. Zhou
Shanghai Key Laboratory of Special Artificial Microstructure and Pohl Institute of Solid State Physics and School of Physics Science and Engineering, Tongji University, Shanghai 200092, China

(Received 26 September 2016; revised manuscript received 16 December 2016; published 13 March 2017)

We report about the anomalous Hall effect in $4f$ $3d$ metallic alloys measured using terahertz time-domain spectroscopy. In this way, we succeeded in revealing ultrafast dynamics of the anomalous Hall effect which accompanies the sub-100-ps optically induced magnetization reversal in a GdFeCo alloy. The experiments demonstrate the ability to control currents at terahertz frequencies in spintronic devices magnetically and ultrafast.

DOI: 10.1103/PhysRevB.95.094418

I. INTRODUCTION

To develop ultrafast spintronics logic protocols for high-speed data processing, one has to find a way to control and detect the spin-dependent transport ultrafast. The conventional approach to study magnetotransport is based on the application of an electrical voltage to a sample and the detection of the subsequent electrical current via electrodes. However, making electrical contacts that transfer a picosecond short signal without substantial distortions and broadening is rather challenging [1]. An elegant solution for the problem of ultrafast conductivity magnetotransport measurements on a sub-pico-second time scale can be found by using freely propagating terahertz waves. As the propagation of terahertz waves in many materials is only affected by the motion of the electrons, it provides arguably the most direct way to probe the magnetotransport properties on an ultrafast time scale.

To date, terahertz spectroscopy has been used to study magnetotransport in a large diversity of materials [2–17]. However, only a few of these studies have been dedicated to magnetically ordered materials and in none of these materials the magnetization could be reversed ultrafast. All-optical magnetization reversal by a single laser pulse is especially an attractive feature for potential spintronic devices, as it indicates the feasibility of both ultrafast and nonvolatile operation, without the need of a permanent bias field. Therefore, to reveal sub-100-ps dynamics of the anomalous Hall effect, we have chosen ferrimagnetic $Gd_x(FeCo)_{1-x}$ thin films, as they are expected to show a significant anomalous Hall effect [18–20], and are known for their ultrafast all-optical magnetization reversal [21–26].

The studied $Gd_x(Fe_{0.875}Co_{0.125})_{1-x}$ samples are 20-nm-thick amorphous films, which have adjacent 5-nm SiN protecting layers and are deposited on a glass substrate using magnetron sputtering. These samples have a ferrimagnetic ordering and an out-of-plane magnetic anisotropy in the studied Gd concentration range ($0.2 < x < 0.3$), with the magnetization being dominated by the FeCo magnetic sublattice at room temperature. At lower temperatures the magnetization of the Gd magnetic sublattice may start to dominate. The temperature at which this happens is known as the magnetization compensation temperature, the value of which can be tuned with the concentration of Gd.

II. STATIC ROOM-TEMPERATURE MEASUREMENTS

Our experimental setup consists of a terahertz time domain spectrometer designed to allow simultaneous excitation of the sample with an intense optical pump and detecting changes in a terahertz probe pulse [see also Fig. 1(a) and the Appendices]. The polarization of the incident terahertz radiation is set by a wiregrid polarizer. Another pair of wiregrid polarizers put after the sample is used to reconstruct the polarization state of the terahertz radiation transmitted through the sample. The sample is situated inside a cryostat with a superconducting magnet. The bias magnetic field is applied along the normal of the sample.

In Fig. 1(b) we show examples of the transmitted terahertz waveforms, measured without the laser pump present, for the $Gd_{0.25}(FeCo)_{0.75}$ sample. The top window of this figure shows the transmission when the terahertz polarizers before and after the sample are oriented parallel. It is clear that the transmitted electric field is time resolved with a sub-pico-second resolution and that applying an external magnetic field of opposite polarity does not induce significant changes to the observed electric field. The lower panel of Fig. 1(b) shows the electric field for the case when the terahertz polarizers before and after the sample are crossed. The difference between the outcomes of the experiments with parallel and crossed polarizers reveals a rotation of the polarization of the terahertz radiation. Both magnetization dependent and magnetization independent

*t.huisman@science.ru.nl

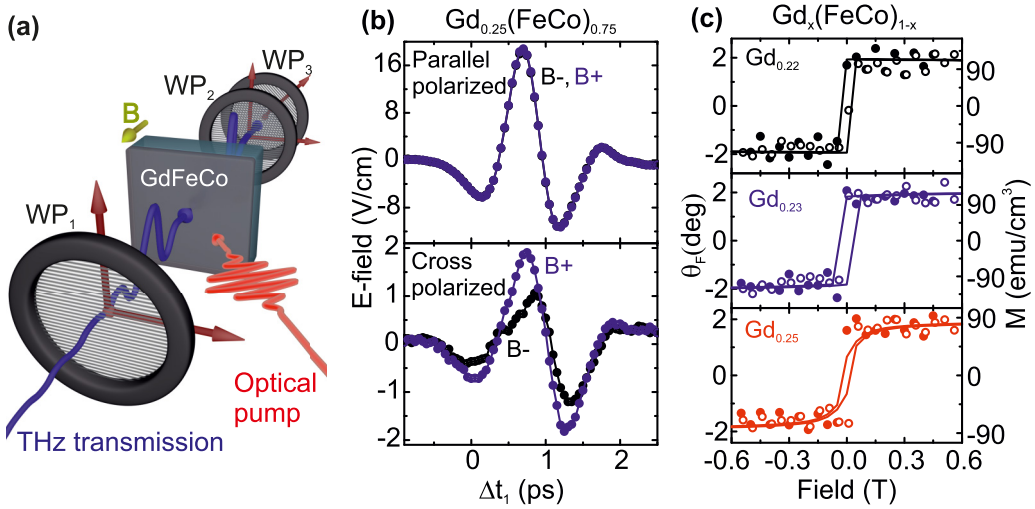

FIG. 1. Schematics and room-temperature measurements. (a) Terahertz radiation is transmitted through GdFeCo films. The wiregrid polarizers WP_1, WP_2, and WP_3 allow for polarization resolved measurements. Additionally an optical pump pulse can be used to change the transport properties of the metallic films. (b) Observed terahertz transmission traces for the $Gd_{0.25}(FeCo)_{0.75}$ sample as a function of time (Δt_1). The top panel shows the transmission when WP1 and WP_2 are parallel to each other, while the lower panel shows the transmission when WP_1 and WP_2 are 90° rotated with respect to each other. WP_3 always stays fixed at 45°. B+ corresponds to an applied field of 0.3 T, and B− corresponds to an applied field of −0.3 T. (c) The dots represent the Faraday rotation at terahertz frequencies for the $Gd_x(FeCo)_{1-x}$ samples, shown as a function of applied field and averaged between 0.5 and 1 THz. The open symbols indicate the data taken with a positive magnetic field sweep direction, while the closed symbols correspond to a negative magnetic field sweep direction. The solid lines are measurements of the magnetization using a vibrating sample magnetometer.

polarization rotations are observed here; the former is ascribed to the Faraday effect in the sample, while the latter arises due to linear dichroism in the windows of the cryostat.

Experimentally we can obtain the Faraday rotation θ_F by determining the absolute rotation as described in Ref. [27], for opposite applied magnetic fields strong enough to saturate the magnetization, taking the difference and dividing by 2. In Fig. 1(c) we show with dots the measured Faraday rotation at terahertz frequencies as a function of field for three different $Gd_x(FeCo)_{1-x}$ samples, without pump present. Every dot represents the mean terahertz rotation averaged between 0.5 and 1 THz, measured for two orthogonal incident polarizations. In the Appendices we show similar measurements for $L1_0\,FePt_{1-x}Pd_x$ films. Only the $Gd_{0.2}(FeCo)_{0.8}$ sample showed a small measurable in-plane anisotropy and magnetic field induced ellipticity. The Faraday rotations of Fig. 1(c) are compared with the solid lines representing the magnetization as measured with a vibrating sample magnetometer (VSM). An appreciable agreement can be found between the two different data sets.

III. THEORETICALLY RELATING THE FARADAY ROTATION AND THE ANOMALOUS HALL EFFECT

In order to gain insight into how the Faraday effect at terahertz frequencies occurs and to make quantitative estimates of it, we consider a thin film which is isotropic in plane and has out-of-plane magnetic anisotropy, parallel to $\hat{\mathbf{z}}$. We also assume the incident radiation propagates parallel to $\hat{\mathbf{z}}$. In this case we can write the relevant permittivity tensor as

$$\boldsymbol{\epsilon} = \begin{pmatrix} \epsilon_{xx} & \epsilon_{xy}(M) \\ -\epsilon_{xy}(M) & \epsilon_{xx} \end{pmatrix}. \tag{1}$$

The eigenvectors of this tensor show that the proper basis is made of left- and right-handed circular polarization, with corresponding refractive indices $n_+ = \sqrt{\epsilon_{xx} + i\epsilon_{xy}}$ and $n_- = \sqrt{\epsilon_{xx} - i\epsilon_{xy}}$. To interpret the experiments, we assume incident linearly polarized light in a Cartesian coordinate system, transform this to circularly polarized light interacting with the medium, and transform the transmitted circularly polarized light to Cartesian coordinates again. In Jones matrix formalism this would look like

$$\begin{aligned} \begin{pmatrix} E'_x \\ E'_y \end{pmatrix} &= \frac{1}{2}\begin{pmatrix} 1 & 1 \\ i & -i \end{pmatrix}\begin{pmatrix} t_+ & 0 \\ 0 & t_- \end{pmatrix}\begin{pmatrix} 1 & -i \\ 1 & i \end{pmatrix}\begin{pmatrix} E_x \\ E_y \end{pmatrix} \\ &= \frac{1}{2}\begin{pmatrix} t_- + t_+ & i(t_- - t_+) \\ -i(t_- - t_+) & t_- + t_+ \end{pmatrix}\begin{pmatrix} E_x \\ E_y \end{pmatrix}, \end{aligned} \tag{2}$$

where E_x and E_y are the incident electric-field components, E'_x and E'_y are the transmitted electric-field components, and t_+ and t_- are the transmission coefficients for circularly polarized waves. Assuming the incident radiation is given by $E_x = 1$ and $E_y = 0$, the Faraday rotation can be represented by [27]

$$\theta_F = \mathrm{Re}\left[\tan^{-1}\left(\frac{E'_y}{E'_x}\right)\right] = \mathrm{Re}\left[\tan^{-1}\left(-i\frac{t_- - t_+}{t_- + t_+}\right)\right], \tag{3}$$

and the magnetization induced ellipticity can be represented by

$$\begin{aligned} \eta &= \frac{\sin^{-1}\left(\tanh\left\{\mathrm{Im}\left[\tan^{-1}\left(\frac{E'_y}{E'_x}\right)\right]\right\}\right)}{2} \\ &= \frac{\sin^{-1}\left(\tanh\left\{\mathrm{Im}\left[\tan^{-1}\left(-i\frac{t_- - t_+}{t_- + t_+}\right)\right]\right\}\right)}{2}. \end{aligned} \tag{4}$$

For optically thick samples the transmission coefficients for a single terahertz pulse would simply be given by multiplying the Fresnel transmission coefficients at the surfaces, and taking into account a phase delay and absorption inside the sample. However, terahertz radiation takes much less than 1 ps to propagate through our metallic films and hence the samples should be regarded as a Fabry-Pérot ethalon. Assuming the wave vector inside the metallic films multiplied with the total thickness of these films to be much smaller than 1, and if the refractive index of the medium is much larger than the ones of the surrounding media, we can write [28]

$$t_{\pm} \approx \frac{2n_1}{(n_1+n_2) - id\frac{\omega}{c}n_{\pm}{}^2}, \tag{5}$$

where n_1 and n_2 are the refractive indices of the surrounding media, ω is the angular frequency, c is the speed of light, and d is the thickness of the film. From the Maxwell equations it can be shown that the permittivity is related to the conductivity by

$$\epsilon(\omega) = \epsilon_{\infty} + \frac{\sigma(\omega)}{\omega}i, \tag{6}$$

where ϵ_{∞} is the frequency independent permittivity, and $\sigma(\omega)$ is the optical conductivity. For metals the conductivity is typically much larger than the frequency independent permittivity. Equation (5) together with the vacuum impedance Z_0 gives in this case

$$t_{\pm} \approx \frac{2n_1}{(n_1+n_2) + Z_0 d(\sigma_{xx} \pm i\sigma_{xy})}, \tag{7}$$

which resembles the commonly used Tinkham equation [29]. We can give the Faraday angle as follows:

$$\begin{aligned}\theta_F &= \mathrm{Re}\left[\tan^{-1}\left(-i\frac{1/t_+ - 1/t_-}{1/t_+ + 1/t_-}\right)\right] \\ &\approx \mathrm{Re}\left(\frac{Z_0 d\sigma_{xy}}{n_1+n_2+Z_0 d\sigma_{xx}}\right),\end{aligned} \tag{8}$$

for which we assumed small rotations as to approximate $\tan^{-1}(x) \approx x$. Similarly, we can write

$$\eta \approx \frac{1}{2}\mathrm{Im}\left(\frac{Z_0 d\sigma_{xy}}{n_1+n_2+Z_0 d\sigma_{xx}}\right). \tag{9}$$

To relate the optical conductivity to the conductivity as measured with dc electronic transport measurements, assumptions have to be made on the movement of electrons. This is most commonly done with the Drude model, also for the transmission measurements at terahertz frequencies. To also account for the anomalous Hall effect, we consider the movement of free electrons as a function of frequency in an xy plane perpendicular to the magnetization described by the following two equations of motion (in the spectral domain):

$$-m\omega^2 x_0 - \frac{m}{\tau}i\omega x_0 - \lambda y_0 = -eE_{x0}, \tag{10}$$

$$-m\omega^2 y_0 - \frac{m}{\tau}i\omega y_0 + \lambda x_0 = -eE_{y0} \tag{11}$$

where m is the electron mass, τ is the scattering time, λ describes the anomalous Hall effect, e is the absolute value of the electron charge, and E_{x0} and E_{y0} are the complex electric-field amplitudes applied along x and y, respectively. Note that for the normal Hall effect $\lambda = i\omega eB$, with B being the externally applied magnetic field. Solving the equation of motions with respect to x_0 and y_0 gives in matrix formalism

$$\begin{aligned}\begin{pmatrix}x_0\\ y_0\end{pmatrix} = &-\frac{e}{\left(-m\omega^2 - \frac{i\omega m}{\tau}\right)^2 + \lambda^2} \\ &\times \begin{pmatrix}-m\omega^2 - \frac{i\omega m}{\tau} & \lambda \\ -\lambda & -m\omega^2 - \frac{i\omega m}{\tau}\end{pmatrix}\begin{pmatrix}E_{x0}\\ E_{y0}\end{pmatrix}.\end{aligned} \tag{12}$$

Our measurements indicate that the longitudinal conductivity at terahertz frequencies is not significantly affected by the anomalous Hall effect for our studied materials. This allows us to approximate

$$\begin{pmatrix}x_0\\ y_0\end{pmatrix} \approx \frac{e}{m\omega^2 + \frac{i\omega m}{\tau}}\begin{pmatrix}1 & -\frac{\lambda}{m\omega^2+\frac{i\omega m}{\tau}} \\ \frac{\lambda}{m\omega^2+\frac{i\omega m}{\tau}} & 1\end{pmatrix}\begin{pmatrix}E_{x0}\\ E_{y0}\end{pmatrix}. \tag{13}$$

The permittivity of the electrons can be expressed in the movement of electrons by $(\boldsymbol{\epsilon} - \epsilon_0)\mathbf{E} = -Ne\mathbf{x}$, where N is the number of electrons in a unit volume, and hence if ϵ_{∞} is small $\boldsymbol{\sigma}\mathbf{E} \approx -\frac{\omega}{i}Ne\mathbf{x}$. This gives

$$\boldsymbol{\sigma} \approx \frac{Ne^2\tau}{m(1-i\omega\tau)}\begin{pmatrix}1 & \frac{i\tau\lambda}{m\omega(1-i\omega\tau)} \\ -\frac{i\tau\lambda}{m\omega(1-i\omega\tau)} & 1\end{pmatrix}. \tag{14}$$

From this, we can see that only if λ is proportional to ω we can get nondiverging off-diagonal conductivity terms for $\omega \to 0$, which physically should be the case. In other words, λ should depend on the velocity of the electrons, similar as for the case of the normal Hall effect. Hence we use a new definition: $i\omega\lambda^* = \lambda$, so that

$$\boldsymbol{\sigma} \approx \frac{Ne^2\tau}{m(1-i\omega\tau)}\begin{pmatrix}1 & -\frac{\tau\lambda^*}{m(1-i\omega\tau)} \\ \frac{\tau\lambda^*}{m(1-i\omega\tau)} & 1\end{pmatrix}. \tag{15}$$

From this we can define the longitudinal conductivity as

$$\sigma_{xx} = \sigma_{xx}(0)\frac{1}{1-i\omega\tau} \tag{16}$$

with

$$\sigma_{xx}(0) = \frac{Ne^2\tau}{m} \tag{17}$$

and the anomalous Hall effect conductivity as

$$\sigma_{xy} = \sigma_{xy}(0)\frac{1}{(1-i\omega\tau)^2} \tag{18}$$

with

$$\sigma_{xy}(0) = \pm\frac{Ne^2\tau^2\lambda^*}{m^2}. \tag{19}$$

It follows that

$$\frac{\sigma_{xy}}{\sigma_{xx}} = \frac{\sigma_{xy}(0)}{\sigma_{xx}(0)}\frac{1}{1-i\omega\tau} \tag{20}$$

and the estimated Faraday rotation and magnetization induced ellipticity in the Drude model for the case when $Z_0 d\sigma_{xx} \gg (n_1+n_2)$ are then given by

$$\theta_F \approx \frac{\sigma_{xy}(0)}{\sigma_{xx}(0)}\frac{1}{1+(\omega\tau)^2}, \tag{21}$$

$$\eta \approx \frac{1}{2}\frac{\sigma_{xy}(0)}{\sigma_{xx}(0)}\frac{\omega\tau}{1+(\omega\tau)^2}. \tag{22}$$

For GdCo and GdFe thin films with a Gd concentration close to 25%, literature reports $\frac{\sigma_{xy}(0)}{\sigma_{xx}(0)}$ to be in the range from 0.02 to 0.04 [18–20], which we confirmed experimentally for the $Gd_{0.25}(FeCo)_{0.75}$ sample (see the Appendices). Since for metals a scattering time in the order of 10 fs is common [30], we can expect to measure a Faraday rotation in the order of 1 or 2 deg and a negligible ellipticity. As is shown and discussed in the previous section, this is exactly what we have retrieved experimentally.

IV. STATIC TEMPERATURE-DEPENDENT MEASUREMENTS

It is known that both magnetotransport and the Faraday effect can show magnetic sublattice sensitivity [28,31–34]. To confirm whether the terahertz Faraday rotation has also magnetic sublattice sensitivity, we performed temperature resolved measurements. In Fig. 2(a) we show with dots the mean Faraday rotation at terahertz frequencies as a function of temperature for the $Gd_{0.25}(FeCo)_{0.75}$ sample. The incident polarization of the terahertz radiation is kept fixed. It is clear that from 250 to 265 K the Faraday rotation changes sign as expected when one of the magnetic sublattices is dominating, while the terahertz transmission (not shown) is nearly independent of temperature between 150 and 300 K. Note that the used alternating field of $+/-0.5$ T is smaller than the coercive fields near the compensation temperature. To resolve the compensation temperature better, we fixed the terahertz polarizers in cross-polarized orientation and scanned the field for different temperatures, resulting in Fig. 2(b). It is clear that between 256 and 260 K the coercive field diverges and the sign of the observed Faraday rotation changes. The seemingly different onset of the compensation temperature as observed in the Faraday rotation and VSM measurements shown in Fig. 2(a) are likely due to the different calibrations of the temperature used in the different experimental setups.

V. LASER INDUCED CHANGES TO THE ANOMALOUS HALL EFFECT

To demonstrate the ultrafast light induced modulation of the anomalous Hall effect, we illuminated the $Gd_{0.25}(FeCo)_{0.75}$ sample with a 50-fs short pump pulse, which has a photon energy of 1.55 eV and a fluence of about 7 mJ/cm^2. We note that this fluence is limited in our case by the cryostat windows absorbing part of this pump light and getting damaged for higher fluences. The top panel of Fig. 3(a) shows the transmitted waveforms of the terahertz radiation just before the arrival moment of the pump pulse on the sample (closed symbols) and 600 ps after the arrival (open symbols). It is seen from the figure that the femtosecond optical excitation does not change significantly the terahertz transmission either for positive or for negative applied magnetic field. However, the lower panel of Fig. 3(a) shows that if we perform the same experiment when the incident and detected terahertz polarizations are cross polarized, both the pump and the field induce changes in the observed waveforms. These data show a clear indication that 600 ps after the arrival time of the pump a noticeable modification of the Faraday effect is observed, which is most pronounced close to the peak of the terahertz electric field.

To investigate the origin of the observed photoinduced changes in the Faraday effect we repeated the terahertz transmission experiment displayed in Fig. 3(a), but now looking at the maximum of the transmitted terahertz waveform and varying the time delay between the arrival of the pump and terahertz pulses to the sample. The top panel of Fig. 3(b) shows the photoinduced signal that is even in applied magnetic field as a function of the pump time delay. It is seen that in the first few picoseconds the pump pulses induce a change in the transmission of about 1% which recovers on a time scale close to 100 ps, as shown in the top panel of Fig. 3(c). The lower panels of Figs. 3(b) and 3(c) show a similar type of experiment, but now for crossed polarizers. Again, we measure the peak of the transmitted terahertz field, scanning the time delay of the pump pulses. We focus on the contribution odd in applied

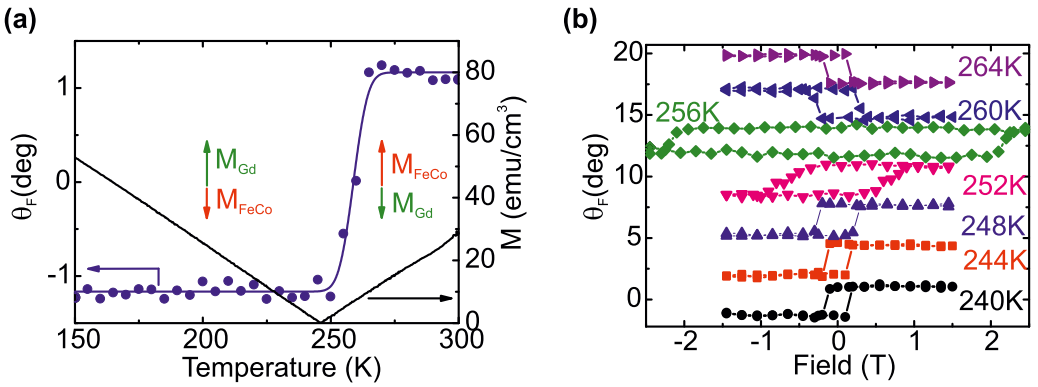

FIG. 2. Temperature dependence of the Faraday rotation at terahertz frequencies for the $Gd_{0.25}(FeCo)_{0.75}$ sample. (a) The Faraday rotation is defined here as the difference in rotation measured for 0.5- and −0.5-T external applied fields, divided by 2 and averaged between 0.5 and 1 THz. The solid black line near the bottom shows the magnetization as measured with a vibrating sample magnetometer, with near zero external applied field. The solid line overlapping the Faraday rotation measurements is a fit used to guide the eye. (b) The peak values of the cross polarized transmission are normalized to give the Faraday rotation as a function of field and temperature. The separate graphs are shifted vertically for clarity.

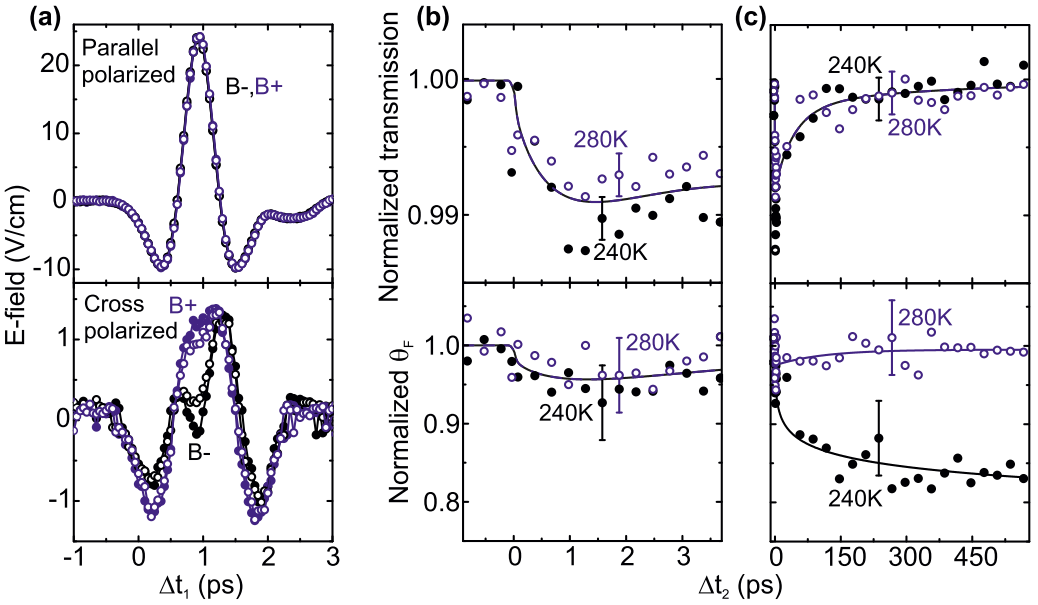

FIG. 3. Pump induced dynamics to the transmission of the terahertz radiation in the $Gd_{0.25}(FeCo)_{0.75}$ sample. (a) The transmission is shown when WP_1 and WP_2 are parallel oriented (top panel) and when they are 90° rotated with respect to each other (lower panel). The blue and black symbols correspond to a 1- and −1-T magnetic field applied, respectively. The closed dots correspond to a pump pulse arriving at the sample 20 ps after the terahertz radiation passes through, while the open dots correspond to a pump pulse arriving at the sample 600 ps before the terahertz radiation is passing through. The sample temperature is set to 235 K. (b) Pump induced dynamics on the peak of the terahertz transmission shown in figure (a) as a function of the difference in arrival time of the terahertz radiation and pump pulses at the sample (Δt_2). The top panel represents the pump induced dynamics in the normal terahertz transmission, while the lower panel represents the pump induced dynamics in the Faraday rotation corresponding to the anomalous Hall effect. The closed black dots correspond to a sample temperature of 240 K, while the open blue dots correspond to a sample temperature of 280 K. (c) Same as (b), but now for a longer time scale. The error bars in (b) and (c) are representative for the estimated standard deviation in these graphs, while the solid lines are fits to guide the eye.

magnetic field that corresponds to the photoinduced change of the Faraday effect. The traces shown in the lower panels of Figs. 3(b) and 3(c) appear to be very similar to typical pump-probe traces used for monitoring ultrafast magnetization dynamics by means of the Faraday effect, but now with the probe at terahertz frequencies.

One can see that on short time scales [lower panel of Fig. 3(b)] both below and above the compensation temperature, there is a fast reduction of the Faraday rotation. This ultrafast dynamics of the Faraday rotation representing the anomalous Hall effect can be due to laser induced dynamics of both electrons and spins. The top panel of Fig. 3(b) indicates that there are laser induced dynamics of the electrons, which changes the transmission of terahertz radiation. However, this makes up for a change of only 1%, while we see in the crossed-polarized configuration a change of a few percent. This indicates that there are likely laser induced dynamics in both the charges and spins.

More clearly, on the time scale of a few hundred picoseconds, the Faraday rotation modulations shown in the lower panel of Fig. 3(c) exhibit distinct dynamics compared to the transient transmission, showing that the changes in the Faraday signal are not purely the consequence of a photoinduced change in the conductivity. The character of the Faraday dynamics changes drastically above and below the magnetization compensation temperature, indicating that the Faraday dynamics is affected by the dynamics in the magnetic ordering. As the Faraday signal represents the anomalous Hall effect, we conclude that this observation represents the photoinduced modification of the anomalous Hall effect due to the magnetization dynamics.

Obviously, after laser excitation the magnetization should relax to one of the metastable states. While above the compensation temperature we observe that the Faraday signal is restored to the initial state on a time scale of a few hundred picoseconds, below the compensation temperature, but on the very same time scale, it is seen that the system relaxes to another magnetic state. The time dependence of the terahertz Faraday signal follows exactly the dynamics expected from laser induced magnetization reversal [22–24,26]. Especially at higher fields, like the ones used here, it can be expected that when the sample is heat driven across the compensation temperature the magnetization should reverse. While this result is expected, previous measurements of laser induced magnetization reversal were done mostly with optical probes, which measure the spin ordering indirectly via electronic transitions. Our experiment with a terahertz Faraday probe is a proof-of-principle demonstration of a more direct probe via intraband transitions. We note that our terahertz probe has a diameter of about 2.5 mm on the sample, while our pump pulses have a diameter which is almost twice as narrow. It can therefore be expected that a full reversal of the magnetization is not shown as a change in the magnetization of 200%, but much less. Taking also into consideration that most likely only close to the middle of the pump spot the magnetization reverses, a change in the cross-polarized terahertz transmission of a few tenths of a percent can indeed be expected.

VI. CONCLUSIONS

To conclude, we have performed a study on the temporal evolution of terahertz spin-dependent transport with sub-pico-second resolution. Particularly, we have measured the polarization state of the terahertz pulse after an interaction with GdFeCo thin films that is connected to the anomalous Hall effect in these materials. The strength of the anomalous Hall effect at terahertz frequencies can be largely reduced by a femtosecond laser excitation on a sub-100-ps time scale. Our experiment mimics sub-100-ps operation of a spin transistor, in which the source-drain voltage is applied from a freely propagating terahertz wave and a femtosecond laser pulse plays the role of the gate by acting on the magnetic ordering. Besides ultrafast and nonvolatile operation, further optimization could make this type of spin transistor energy efficient [24]. Our proof-of-principle experiment demonstrates the feasibility to reveal the fundamental and practical limitations on the speed of magnetic control of conductivity and thus to define the ultimate speed for the operation of spintronic devices.

ACKNOWLEDGMENTS

We would like to thank T. Toonen and S. Semin for technical support. This work was supported by the Foundation for Fundamental Research on Matter, the European Unions Seventh Framework Program (FP7/2007-2013) Grants No. 280555 (Go-Fast) and No. 281043 (FemtoSpin), European Research Council Grants No. 257280 (Femtomagnetism) and No. 339813 (Exchange), the program Leading Scientist of the Russian Ministry of Education and Science (14.Z50.31.0034), the State Key Project of Fundamental Research Grant No. 2015CB921501, and the National Science Foundation of China Grants No. 51331004 and No. 51501131.

APPENDIX A: EXPERIMENTAL SETUP

The experimental setup is shown in Fig. 4 and consists of a terahertz time domain spectrometer combined with intense optical pump pulses. Terahertz pulses are generated using a 1-mm-thick ZnTe crystal, providing terahertz radiation in a range from about 0.1 to 3 THz. The polarization of this terahertz radiation is fixed by a wiregrid polarizer. Two gold coated parabolic mirrors collect and refocus the terahertz radiation onto a sample. Simultaneously, a small hole in one of the parabolic mirrors allows an intense pump pulse to be incident on the sample. After the sample a second set of parabolic mirrors collects and refocuses the terahertz radiation through two wiregrid polarizers, allowing us to reconstruct the terahertz waveform polarization resolved. A third pair of parabolic mirrors is used to collect and refocus the terahertz radiation onto a second 1-mm-thick ZnTe crystal which is optically gated by a laser pulse. The terahertz radiation induces birefringence by means of the Pockels effect, resulting in terahertz-induced ellipticity to the laser pulses used for optical gating. Measuring this ellipticity using a quarter-wave plate and a polarization balanced detection scheme allows reconstruction of the electric field of the terahertz pulse in time. The terahertz radiation is focused onto the sample in a spot size of a few millimeters in diameter. So any external magnet used for applying fields out of plane needs to have a hole or a transparent

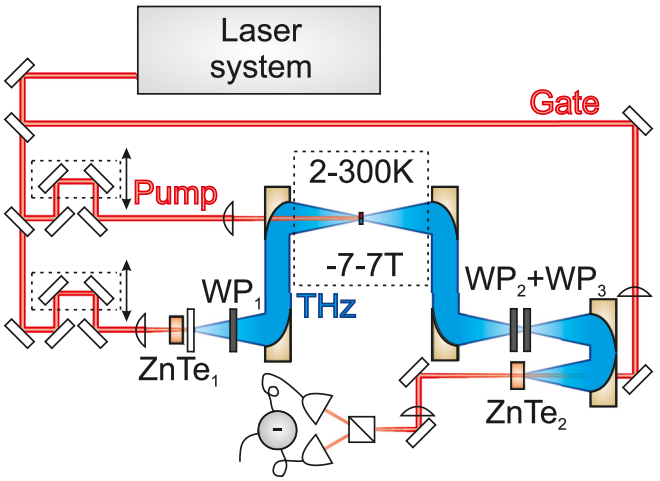

FIG. 4. Schematics of the experimental setup employed. Laser pulses from the amplified titanium-sapphire laser system are split in three: a pump, a terahertz generation, and a gate. Terahertz radiation is generated using a ZnTe crystal ($ZnTe_1$) and polarization filtered with a wiregrid polarizer (WP_1). This terahertz radiation is transmitted through the sample situated inside a superconducting 7-T cryostat. The transmitted radiation is measured polarization resolved with wiregrid polarizers (WP_2+WP_3) and using the gate pulses for electro-optic sampling. The transmission of the sample can be optically modulated using the pump pulses.

region at terahertz frequencies of at least a few millimeters close to the sample up to a few centimeters further away from the sample. To this end, we make use of a superconducting 7-T cryostat, which fits this requirement and simultaneously allows tuning the temperature of the sample. Further, to prevent

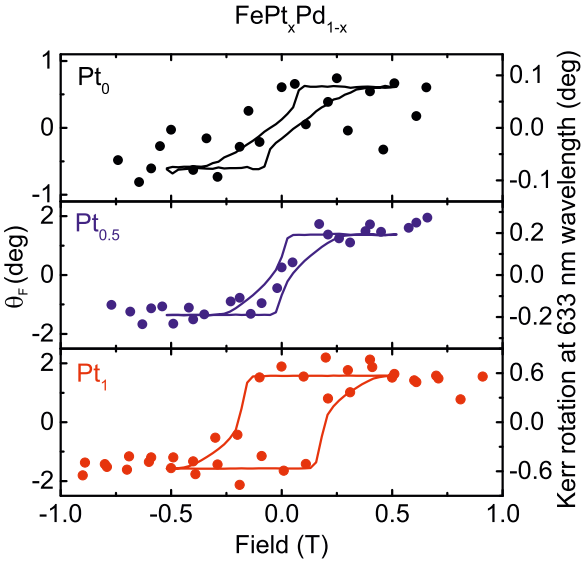

FIG. 5. Faraday rotation measured at terahertz frequencies and at room temperature of the $FePt_{1-x}Pd_x$ samples. The dots represent the Faraday rotation averaged between 0.5 and 1 THz. The solid lines are magneto-optical Kerr rotation measurements performed with a helium-neon laser.

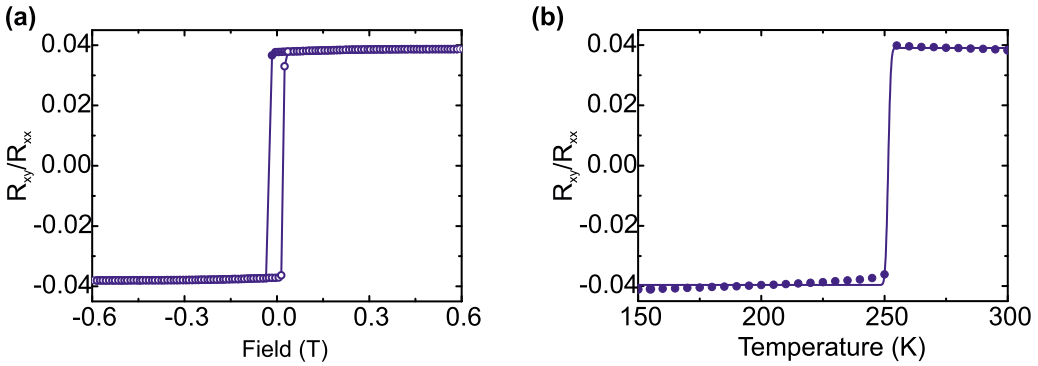

FIG. 6. The dc anomalous Hall effect measurements of the $Gd_{0.25}(FeCo)_{0.75}$ sample. (a) The dots represent the anomalous Hall resistance R_{xy} normalized to the sheet resistance R_{xx}, shown as a function of applied field at a temperature of 300 K. The open symbols indicate the data taken with a positive magnetic field sweep direction, while the closed symbols correspond to a negative magnetic field sweep direction. (b) The normalized anomalous Hall effect resistance measured and averaged for 0.5- and −0.5-T external applied fields, as a function of temperature. The solid line overlapping the measurement is a fit used to guide the eye.

absorption of terahertz radiation due to the water in the air, we put the full setup in a nitrogen flushed purging box.

APPENDIX B: TERAHERTZ FARADAY MEASUREMENT $L1_0$ $FePt_{1-x}Pd_x$ FILMS

We also performed measurements on 20-nm-thick $L1_0$ $FePt_{1-x}Pd_x$ films, with static properties which were characterized before [35,36]. These samples are deposited on single crystal MgO(001) substrates by magnetron sputtering. The studied $FePt_{1-x}Pd_x$ films are ferromagnetic ordered samples with a saturation magnetization of about 1100 emu/cm^3, a coercive field up to 0.4 T at room temperature, and out-of-plane magnetic anisotropy.

In Fig. 5, we show with dots the measured Faraday rotation at terahertz frequencies as a function of field for three different $FePt_{1-x}Pd_x$ samples, without pump present. Every dot represents a time-resolved terahertz transmission trace, from which we took the mean rotation between 0.5 and 1 THz. Every Faraday rotation measurement was taken for two different orthogonal incident polarizations and two different orthogonal transmitted polarizations, which indicated that the samples could be regarded as in-plane isotropic. These Faraday rotations are compared with the solid lines representing the magneto-optical Kerr effect measured at a wavelength of 633 nm. For $FePt_{0.5}Pd_{0.5}$ and FePt there seems to be a clear correlation between the two different data sets, especially regarding the coercive field. However, for FePd the magnetization induced Faraday rotation at terahertz frequencies is close to the fluctuations in the data points. As shown in Ref. [35] the ratio between the anomalous Hall effect resistivity and longitudinal resistivity varies dramatically from a Pt concentration of zero to 0.65, but for higher concentrations the apparent change of this ratio is smaller. It seems therefore reasonable that the Faraday rotations observed for $FePt_{0.5}Pd_{0.5}$ and FePt are comparable to each other, and larger than observed for FePd.

APPENDIX C: ELECTRONIC TRANSPORT MEASUREMENTS OF $Gd_{0.25}(FeCo)_{0.75}$

After performing our terahertz Faraday experiments on the $Gd_{0.25}(FeCo)_{0.75}$ sample, we used the van der Pauw method in order to measure the dc sheet and Hall resistance (R_{xx} and R_{xy}, respectively), as shown in Fig. 6. This figure shows that the field and temperature dependence of the anomalous Hall resistance is comparable to the terahertz Faraday measurements. Moreover, since the width and length of our sample are equal to each other, we can take R_{xy}/R_{xx} equal to σ_{xy}/σ_{xx}, showing that $\sigma_{xy}/\sigma_{xx} \approx 0.04$, consistent with the literature [18–20].

[1] Z. Zhong, N. M. Gabor, J. E. Sharping, A. L. Gaeta, and P. L. McEuen, Terahertz time-domain measurement of ballistic electron resonance in a single-walled carbon nanotube, Nat. Nanotechnol. **3**, 201 (2008).

[2] B. Parks, S. Spielman, and J. Orenstein, High-frequency Hall effect in the normal state of $YBa_2Cu_3O_7$, Phys. Rev. B **56**, 115 (1997)

[3] R. Shimano, Y. Ino, Yu. P. Svirko, and M. Kuwata-Gonokami, Terahertz frequency Hall measurement by magneto-optical Kerr spectroscopy in InAs, Appl. Phys. Lett. **81**, 199 (2002)

[4] O. Morikawa, A. Quema, S. Nashima, H. Sumikura, T. Nagashima, and M. Hangyo, Faraday ellipticity and Faraday rotation of a doped-silicon wafer studied by terahertz time-domain spectroscopy, J. Appl. Phys. **100**, 033105 (2006)

[5] K. J. Chau and A. Y. Elezzabi, Photonic Anisotropic Magnetoresistance in Dense Co Particle Ensembles, Phys. Rev. Lett. **96**, 033903 (2006)

[6] K. J. Chau, M. Johnson, and A. Y. Elezzabi, Electron-Spin-Dependent Terahertz Light Transport in Spintronic-Plasmonic Media, Phys. Rev. Lett. **98**, 133901 (2007)

[7] I. Crassee, J. Levallois, A. L. Walter, M. Ostler, A. Bostwick, E. Rotenberg, T. Seyller, D. van der Marel, and A. B. Kuzmenko, Giant Faraday rotation in single- and multilayer graphene, Nat. Phys. **7**, 48 (2011)

[8] R. Shimano, Y. Ikebe, K. S. Takahashi, M. Kawasaki, N. Nagaosa, and Y. Tokura, Terahertz Faraday rotation induced by an anomalous Hall effect in the itinerant ferromagnet $SrRuO_3$, Europhys. Lett. **95**, 17002 (2011)

[9] R. Valdés Aguillar, A. V. Stier, W. Liu, L. S. Bilbro, D. K. George, N. Bansal, L. Wu, J. Cerne, A. G. Markelz, S. Oh, and N. P. Armitage, Terahertz Response and Colossal Kerr Rotation from the Surface States of the Topological Insulator Bi_2Se_3, Phys. Rev. Lett. **108**, 087403 (2012)

[10] A. M. Shuvaev, G. V. Astakhov, A. Pimenov, C. Brüne, H. Buhmann, and L. W. Molenkamp, Giant Magneto-Optical Faraday Effect in HgTe Thin Films in the Terahertz Spectral Range, Phys. Rev. Lett. **106**, 107404 (2011)

[11] C. J. E. Straatsma, M. Johnson, and A. Y. Elezzabi, Terahertz spinplasmonics in random ensembles of Ni and Co microparticles, J. Appl. Phys. **112**, 103904 (2012)

[12] M. Shalaby, M. Peccianti, Y. Ozturk, and R. Morandotti, A magnetic non-reciprocal isolator for broadband terahertz operation, Nat. Commun. **4**, 1558 (2013)

[13] Y. Lubashevsky, L. Pan, T. Kirzhner, G. Koren, and N. P. Armitage, Optical Birefringence and Dichroism of Cuprate Superconductors in the THz Regime, Phys. Rev. Lett. **112**, 147001 (2014)

[14] J. N. Heyman, R. F. Foo Kune, B. A. Alebachew, M. D. Nguyen, and J. T. Robinson, Ultrafast terahertz Faraday rotation in graphene, J. Appl. Phys. **116**, 214302 (2014)

[15] T. J. Huisman, R. V. Mikhaylovskiy, A. V. Telegin, Y. P. Sukhorukov, A. B. Granovsky, S. V. Naumov, T. Rasing, and A. V. Kimel, Terahertz magneto-optics in the ferromagnetic semiconductor $HgCdCr_2Se_4$, Appl. Phys. Lett. **106**, 132411 (2015)

[16] Z. Jin, A. Tkach, F. Casper, V. Spetter, H. Grimm, A. Thomas, T. Kampfrath, M. Bonn, M. Kläui, and D. Turchinovich, Accessing the fundamentals of magnetotransport in metals with terahertz probes, Nat. Phys. **11**, 761 (2015)

[17] K. N. Okada, Y. Takahashi, M. Mogi, R. Yoshimi, A. Tsukazaki, K. S. Takahashi, N. Ogawa, M. Kawasaki, and Y. Tokura, Terahertz spectroscopy on Faraday and Kerr rotations in a quantum anomalous Hall state, Nat. Commun. **7**, 12245 (2016)

[18] M. Hartmann and T. R. McGuire, Relationship between Faraday Rotation and Hall Effect in Amorphous Rare-Earth-Transition-Metal Alloys, Phys. Rev. Lett. **51**, 1194 (1983)

[19] T. Stobiecki, K. Kowalski, and Z. Obuszko, Charge Transfer and Hall Effect in Amorphous GdCo, GdCoMo and GdFe Films, Physica B **130**, 94 (1985)

[20] S. Honda, M. Nawate, M. Ohkoshi, and T. Kusuda, Hall effect and magnetic properties in GdFe and CoCr sputtered films, J. Appl. Phys. **57**, 3204 (1985)

[21] C. D. Stanciu, F. Hansteen, A. V. Kimel, A. Kirilyuk, A. Tsukamoto, A. Itoh, and T. Rasing, All-Optical Magnetic Recording with Circularly Polarized Light, Phys. Rev. Lett. **99**, 047601 (2007)

[22] K. Vahaplar, A. M. Kalashnikova, A. V. Kimel, D. Hinzke, U. Nowak, R. Chantrell, A. Tsukamoto, A. Itho, A. Kirilyuk, and T. Rasing, Ultrafast Path for Optical Magnetization Reversal via a Strongly Nonequilibrium State, Phys. Rev. Lett. **103**, 117201 (2009)

[23] I. Radu *et al.*, Transient ferromagnetic-like state mediating ultrafast reversal of antiferromagnetically coupled spins, Nature (London) **472**, 205 (2011)

[24] M. Savoini *et al.*, Highly efficient all-optical switching of magnetization in GdFeCo microstructures by interference-enhanced absorption of light, Phys. Rev. B **86**, 140404 (2012)

[25] C. E. Graves *et al.*, Nanoscale spin reversal by non-local angular momentum transfer following ultrafast laser excitation in ferrimagnetic GdFeCo, Nat. Mater. **12**, 293 (2013)

[26] Y. Hashimoto *et al.*, Ultrafast time-resolved magneto-optical imaging of all-optical switching in GdFeCo with femtosecond time-resolution and a μm spatial-resolution, Rev. Sci. Instrum. **85**, 063702 (2014)

[27] C. M. Morris, R. V. Aguilar, A. V. Stier, and N. P. Armitage, Polarization modulation time-domain terahertz polarimetery, Opt. Express **20**, 12303 (2012)

[28] T. J. Huisman, R. V. Mikhaylovskiy, A. Tsukamoto, T. Rasing, and A. V. Kimel, Simultaneous measurements of terahertz emission and magneto-optical Kerr effect for resolving ultrafast laser-induced demagnetization dynamics, Phys. Rev. B **92**, 104419 (2015)

[29] M. Tinkham, Energy Gap Interpretation of Experiments on Infrared Transmission through Superconducting Films, Phys. Rev. **104**, 845 (1956)

[30] M. Fox, *Optical Properties of Solids*, 2nd ed. (Oxford University, Oxford, 2010)

[31] Y. Mimura, N. Imamura, and Y. Kushiro, Hall effect in rare-earth-transition-metal amorphous alloy films, J. Appl. Phys. **47**, 3371 (1976)

[32] T. R. McGuire, R. J. Gambino, and R. C. Taylor, Hall effect in amorphous thin-film magnetic alloys, J. Appl. Phys. **48**, 2965 (1977)

[33] A. K. Zvezdin and V. A. Kotov, *Modern Magnetooptics and Magnetooptical Materials*, 1st ed. (Institute of Physics, New York, 1997)

[34] A. R. Khorsand, M. Savoini, A. Kirilyuk, A. V. Kimel, A. Tsukamoto, A. Itoh, and Th. Rasing, Element-Specific Probing of Ultrafast Spin Dynamics in Multisublattic Magnets with Visible Light, Phys. Rev. Lett. **110**, 107205 (2013)

[35] P. He, L. Ma, Z. Shi, G. Y. Guo, J.-G. Zheng, Y. Xin, and S. M. Zhou, Chemical Composition Tuning of the Anomalous Hall Effect in Isoelectronic $L1_0FePd_{1-x}Pt_x$ Alloy Films, Phys. Rev. Lett. **109**, 066402 (2012)

[36] P. He, X. Ma, J. W. Zhang, J. W. Zhang, H. B. Zhao, G. Lüpke, Z. Shi, and S. M. Zhou, Quadratic Scaling of Intrinsic Gilbert Damping with Spin-Orbital Coupling in $L1$FePdPt Films: Experiments and *Ab Initio* Calculations, Phys. Rev. Lett. **110**, 077203 (2013)